Numerical Simulation of the Scattering by S-Shape Surfaces

Leo C. Kempel and John L. Volakis

November 1990

Northrop Corporation
8900 E. Washington Blvd.
Pico Rivera, CA 90660-3737

Numerical Simulation of the Scattering by S-Shape Surfaces

Leo C. Kempel and John L. Volakis

November 1990

Abstract

When an S-shaped surface posseses no derivative discontinuities, techniques such as the Geometrical Theory of Diffraction are not applicable. However, if the radius of curvature is relatively large at every point on the surface, the physical optics approach may be employed. Previously, a Uniform Physical Optics (UPO) solution was presented for this class of surfaces. This report provides a validationof the UPO solution on the basis of a numerical model of the S-shaped surface. It is found that the UPO solution is quite accurate in the specular and non-specular regions for backscatter computations and is also acceptable for bistatic computations in regions where whispering gallery modes are not present. However, the same numerical model was not found suitable for scattering computations by S-shaped non-symmetric surfaces possessing small surface discontinuities unless a higher order model is employed.

1 Introduction

Of interest in this study is a characterization of the scattering by a class of smooth surfaces possessing an inflection point at which the radius of curvature is infinite (see Fig. 1). This belongs to a special class of convex-concave surfaces and recently several asymptotic studies have appeared in the literature for an evaluation of the scattering by these surfaces. As can be expected, these studies have concentrated on the evaluation of the scattering in the nonspecular or shadowed region[1, 2] which is characterized as the region with no geometrical optics returns. Of particular concern has also been the development of a uniform solution which remain valid in the transition region, (i.e. the region near the shadow boundary separating the specular and nonspecular regions). Recently, Pathak and Liang [3] presented such a solution that overcomes the limitations of earlier uniform solutions [4, 5, 6]. All these asymptotic solutions are based on a physical optics approximation of the surface current distribution and the aforementioned papers have only been directed at the evaluation of the physical optics integral. Interestingly, the accuracy of the physical optics approximation has not been addressed apart from its well known failure when multiple reflections or whispering gallery modes are present.

In view of the above, a primary goal in this study is an assessment of the accuracy of the physical optics approximation by comparison with numerical data based on time and frequency domain solutions of suitable models with the previously presented UPO formulation [7]. Generally, it is shown that the physical optics approximation is acceptable for computations in the specular and non-specular regions wherever multiple ray field interactions are absent.

The following section contains a description of the numerical scattering models and a presentation of results based on the numerical and high frequency simulations of the scattering surface. The final section of this report is a discussion on the validity and practical use of the physical optics approximation in modelling the scattering by S-shaped surfaces.

2 Numerical Simulation

The presented uniform physical optics (UPO) solution is only an approximation to the scattering by the S-shape geometry. It is therefore of interest

to examine the accuracy of the UPO solution and, if possible, provide some guidelines for its range of validity. As already mentioned, the UPO solution will certainly fail for observations at bistatic angles where there are contributions due to multiple reflections.

To examine the accuracy of the UPO solution for the S-shape geometry given in figure 1 we considered two numerical models. These are shown in figure 2 and were chosen to isolate the scattering from the front S-shape surface. Looking at figure 2a, on the assumption that $\frac{\pi}{2} < \phi, \phi_o < \pi$ and provided there are no derivative discontinuities at the points e and f, the rear smooth portion of the surface (to the right of e) will not be a scattering contributor. Of course, in order to isolate the scattering from the front portion of the S-shape geometry, it is also necessary to eliminate any contributions from diffractions by the front edge b and the loaded section $f - g$. The separation of these individual contributions can only be accomplished by calculating the time domain response of the entire geometry. This was done by inverse Fourier transforming its frequency response (obtained via a standard code) over a band from 100 MHz to 10 GHz and multiplying it by the lowpass Kaiser based window illustrated in figure 3 to eliminate Gibbs' phenomenon.

Typical backscatter time domain responses of the geometry in figure 2a are shown in figure 4. The one in fig. 4a corresponds to an angle of incidence and observation of $\phi = \phi_o = 110$ degrees (specular region; in the backscatter case the shadow boundary coincides with the normal to the inflection point at d) with the S-shape curve given by the error function

$$y = f(x) = A\, erf(cx) = \frac{2}{\sqrt{\pi}} A \int_0^{cx} e^{-t^2} dt \qquad (1)$$

For the data in figure 4, $A = -.1$, $c = 6$ and the x components of the points b, c, d, e and f are -0.5 m, -0.5 m., 0 m. and 0.5 m., 0.5 m., respectively, with the rear S-shape surface being the image of the front about the axis through the midpoint between e and f. In addition, the section from f to g is occupied by a tapered resistive card whose profile will be discussed later. Four distinct contributions are observed in the illustrated time response and from the left to the right these are respectively associated with the edge at b, the two reflections from above and below the inflection point d and the rear section to the right of the point e. The range profile or time response corresponding to $\phi = \phi_o = 150$ degrees is shown in figure 4b. In this case,

the observation angle is in the non-specular region and the only contribution from the S-shape geometry appears to emanate from the inflection point *d*. It is clear from a comparison of figures 4a and 4b that the response of the S-shape surface has a much lower frequency content in the non-specular region than it does in the specular one. This is also true for the response of the rear section (to the right of *e*) since the resistive card behaves more like a sharp metallic edge at low frequencies.

The procedure for obtaining the isolated backscatter range response of the S-shape section extending from *c* to *e* without any other interference is now straightforward. The time responses at each backscatter angle are range-gated to remove any contributions from the edge at *b* and the rear section of the model. The resulting range-gated response corresponding to that in figure 4b are given in figure 5 and when this is inverse transformed for each incidence angle we obtain the backscatter frequency response at 5 GHz (middle of the frequency window) shown in figure 6. As seen, this is in complete agreement with the UPO solution given by [7, (15)] in conjunction with [7, (17)]. Interestingly, near grazing angles there is no return predicted by the numerical or UPO solution and it is therefore concluded that the frequency content of the range response in figure 5 must be restricted to low frequencies (below 2 GHz for this case study).

The generation of the frequency domain data required for constructing the time or range response is obviously a computationally intensive process. It is therefore desirable to numerically compute the scattering attributed to the S-shape portion of the surface directly in the frequency domain. A suitable model for accomplishing this is illustrated in figure 2b which incorporates another tapered resistive card to suppress the scattering by the front edge at b as was done for the rear edge. Referring to figure 7, it is seen that the chosen tapered resistive card which was also used to terminate the rear section is an acceptable termination for frequencies above 2 GHz. This is also validated from a comparison of the backscatter patterns based on the two numerical models as shown in figure 8. Clearly the pattern obtained by an inverse transformation of the range-gated profile is in good agreement with that obtained by a direct calculation in the frequency domain using the model of figure 2b. Thus, by choosing suitable tapered resistive card terminations it is not necessary to resort to a time domain solution for isolating the scattering by a given S-shape surface.

Using the model in figure 2b we can now proceed with an examination of

the accuracy of the UPO solution as a function of the slope and height of the S-shape surface without excessive computational effort. We found the surface generating function given by (1) particularly attractive for this purpose and figures 9-14 include several comparisons of H-polarization backscatter patterns based on the numerical and UPO solutions. These comparisons reveal that the UPO solution is quite accurate for backscatter calculations provided the minimum radius of curvature (MRC) at any point of the surface is less than 0.5λ. For this case the S-shape surface resembles a step function and the PO approximation is obviously no longer valid. Comparisons of E-polarization bistatic patterns (E- and H-polarization patterns are identical(see [7])) are given in figures 15 and 16 and it is again observed that the numerical data are in good agreement with the UPO solution when the existence region of the whispering gallery modes is excluded. We remark that the numerical model used to generate the E-polarization data was that illustrated in figure 2b and the resistivity profile of the front and back card is given in figure 7 with $R = 60Z_o$.

It should also be noted that in generating the patterns in figures 9-16 care must be exercised to maintain symmetric sampling about the inflection point. If not, because of the rapidly varying phase of the current(see fig. 17), errors will result in the numerical evaluation of the radiation integral. This is demonstrated in figure 18 where we compare patterns based on symmetric and non-symmetric sampling about the inflection point. Clearly, non-symmetric sampling may cause substantial errors near grazing where backscatter is low.

3 Concluding Remarks

In this study, we presented a Uniform Physical Optics solution for scattering by S-shaped surfaces. A corresponding numerical model for the S-shaped surface was also presented for validating the UPO solution. It was found that the UPO solution was remarkably accurate for computations in the backscatter region and for bistatic computations provided no whispering gallery mode effects were present. Future work will entail an examination of the effects associated with derivative discontinuities in the S-shaped surface. The importance of these returns will be quantified by applying range gating. Comparison will be performed with the analysis given in [8].

MISSING
PAGE

References

[1] H. Ikuno and L.B. Felson. Real and complex rays for scattering from a target with inflection points. *Radio Sci.*, 20(2):952–958, Nov. 1987.

[2] H. Ikuno and L.B. Felson. Complex ray interpretation of reflection from concave- complex surfaces. *IEEE Trans. Antennas Propagat.*, 36:1260–1271, Sept. 1988.

[3] P.H. Pathak and M.C. Liang. On a uniform asymptotic solution valid across smooth caustics of rays reflected by smoothly indented boundaries. *IEEE Trans. Antennas Propagat.*, 38:1192–1203, Aug. 1990.

[4] N.C. Albertsen, P. Balling, and N.E. Jensen. Caustics and caustic corrections to the field diffracted by a curved edge. *IEEE Trans. Antennas Propagat.*, 35:297–303, May 1977.

[5] Y.A. Kravtsov. A modification of the geometrical optics method. *Radiofizika*, 7:664–673, 1964.

[6] D. Ludwig. Uniform asymptotic expansion at a caustic. *Commun. Pure Appl. Math.*, XIX:215–250, 1966.

[7] J. L. Volakis, L.C. Kempel, and T.B.A Senior. A Uniform Physical Optics Solution for Scattering by S-shaped Surfaces, University of Michigan Technical Report No. 390285-2-T, 1990.

[8] L. Kaminetsky and J.B. Keller. Diffraction coefficients for higher order edges and vertices. *SIAM J. Appl. Math.*, 22:109–134, 1972.

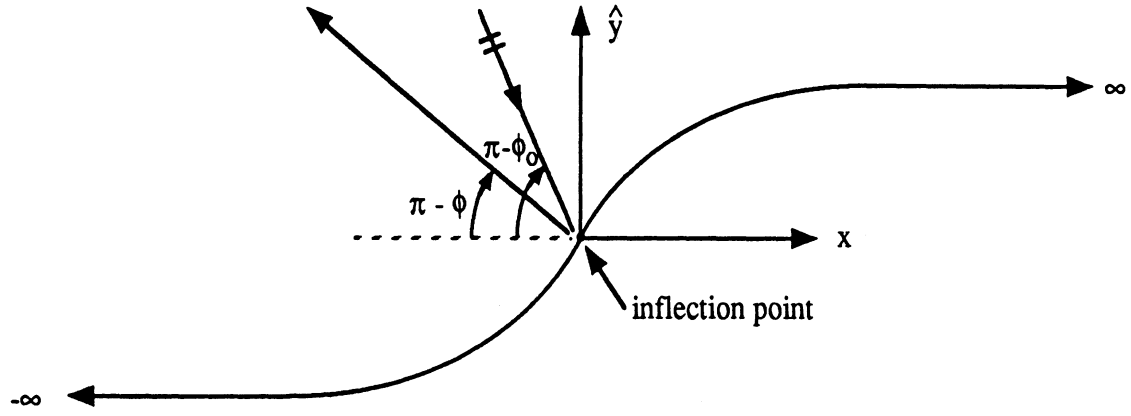

Fig. 1a. Geometry of the S-shape surface.

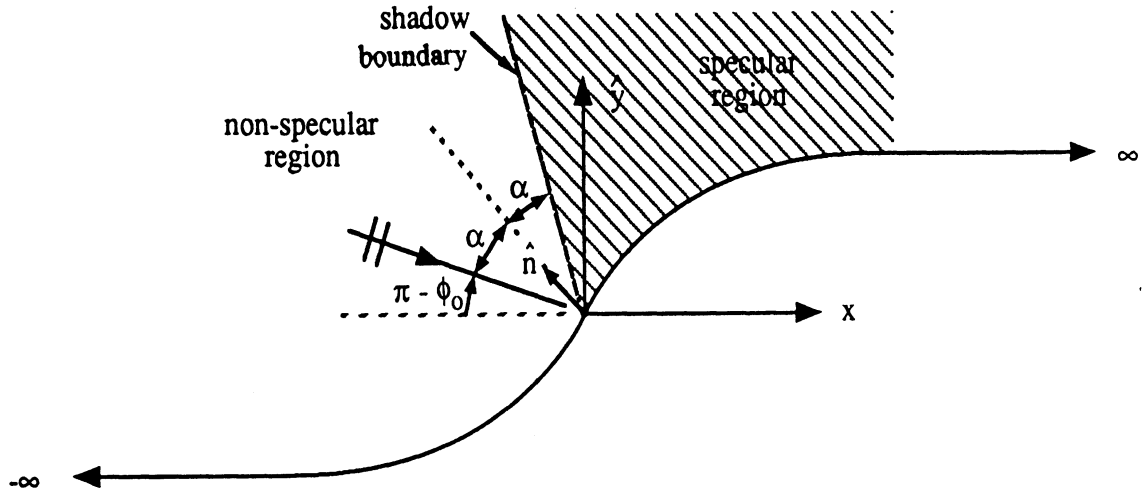

Fig. 1b. Definition of the shadow boundary.

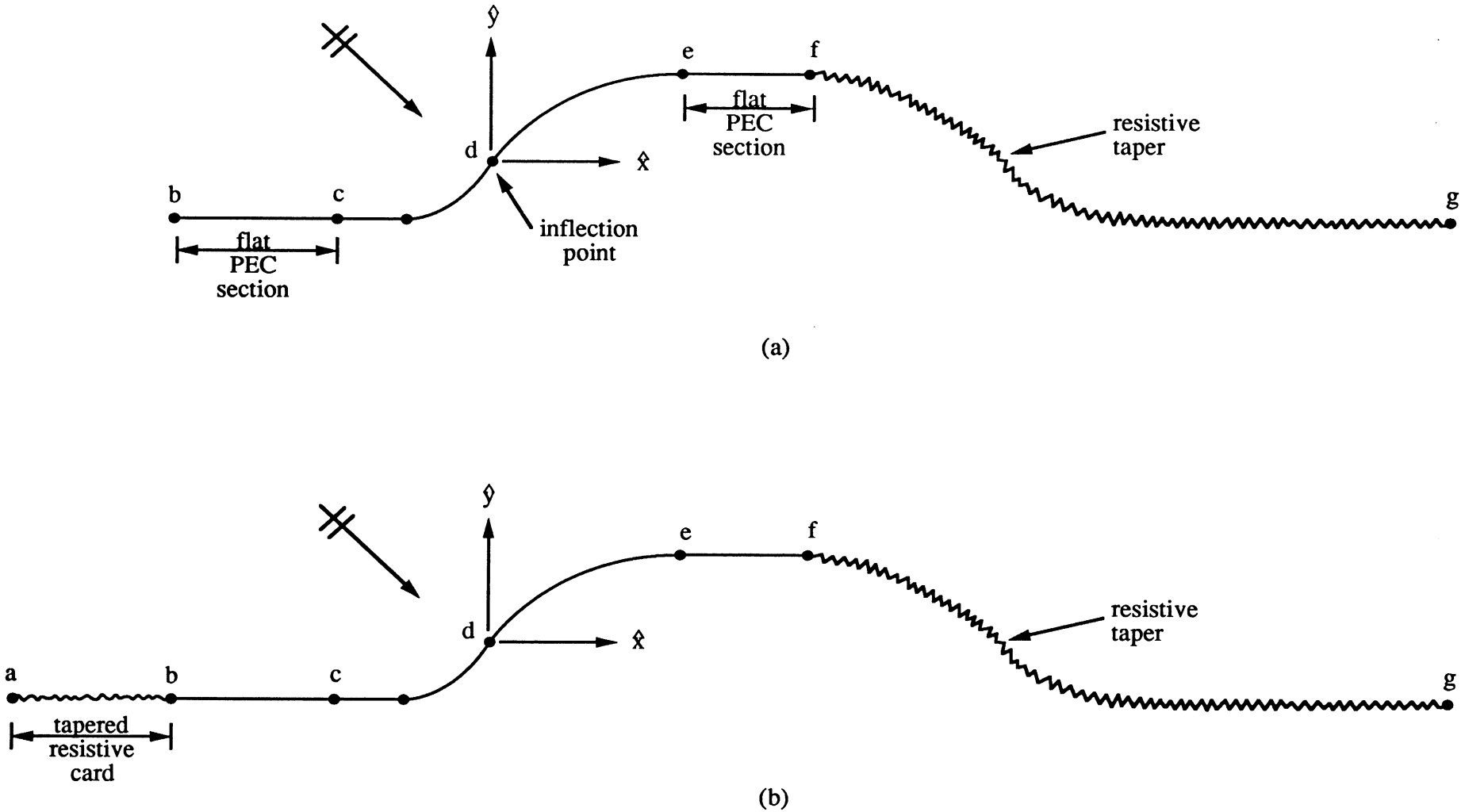

Fig. 2. Numerical models of the S-shape surface
(a) without tapered resistive card in front
(b) with tapered resistive card in front.

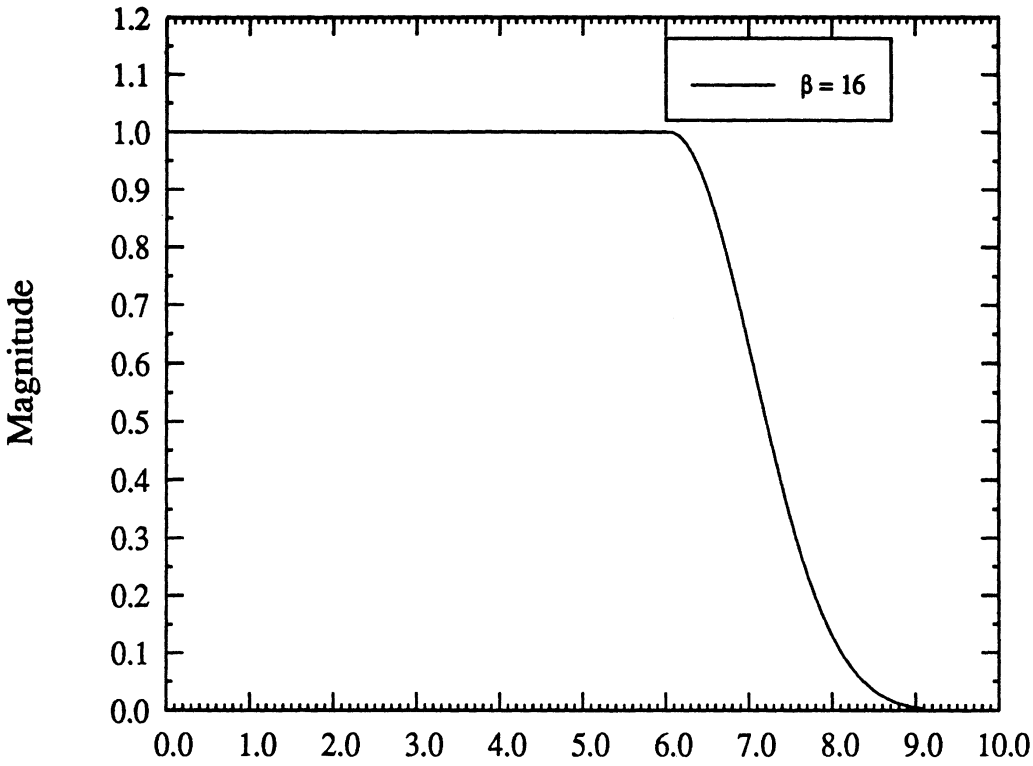

General Kaiser Window or taper formula:

$$\frac{I_o\left(\beta\sqrt{1-r^2}\right)}{I_o(\beta)}$$

$r = (f - f_s)/(f_e - f_s) \qquad f_s < f < f_e$

I_o: Modified Bessel function

β: Control parameter

Fig. 3. Illustration and definition of the Kaiser Window function.

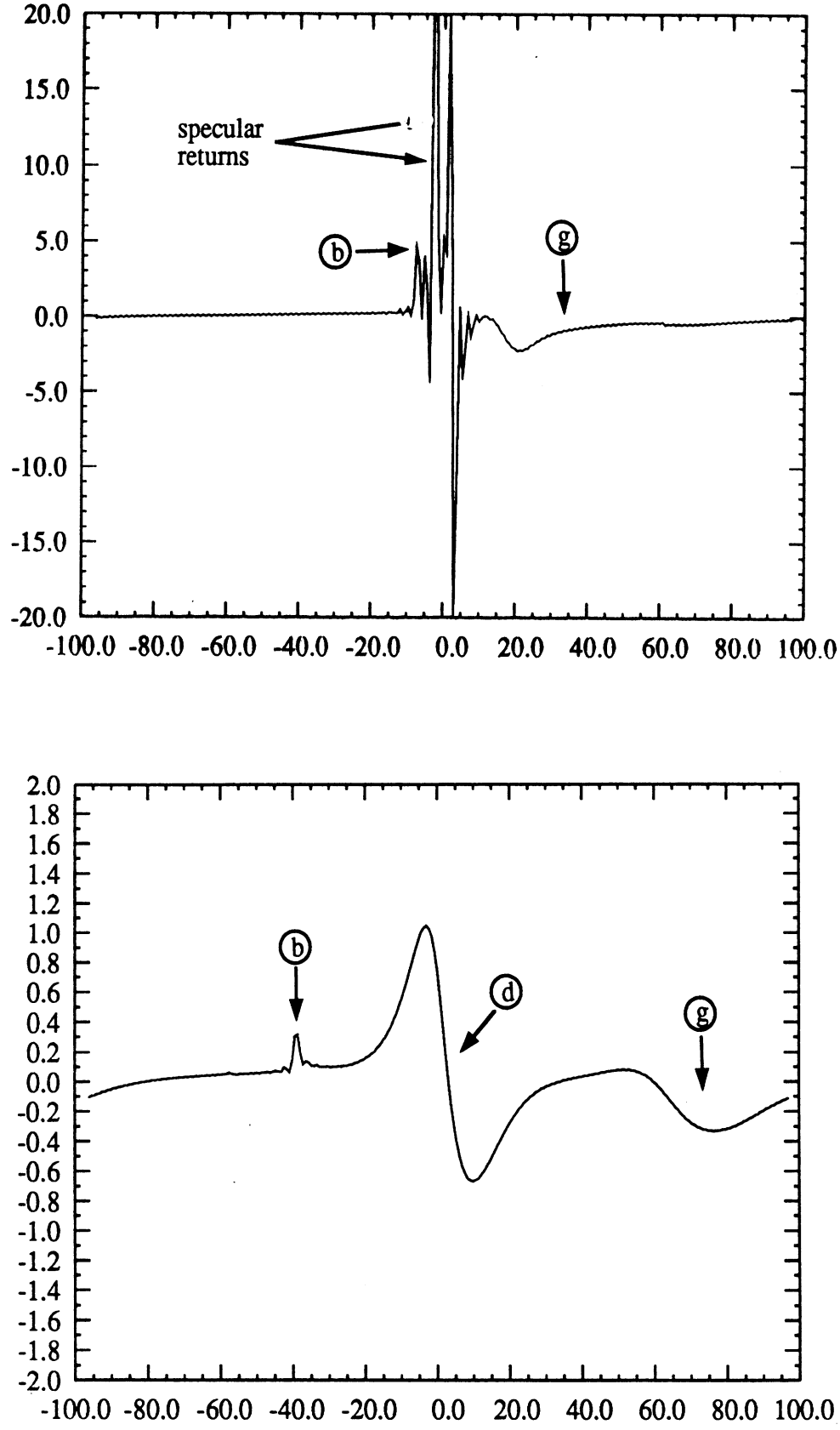

Figure 4. Time response or range profiltes of the geometry in figure 2a (H-polarization).
(a) $\phi = \phi_o = 110°$ (b) $\phi = \phi_o = 150°$

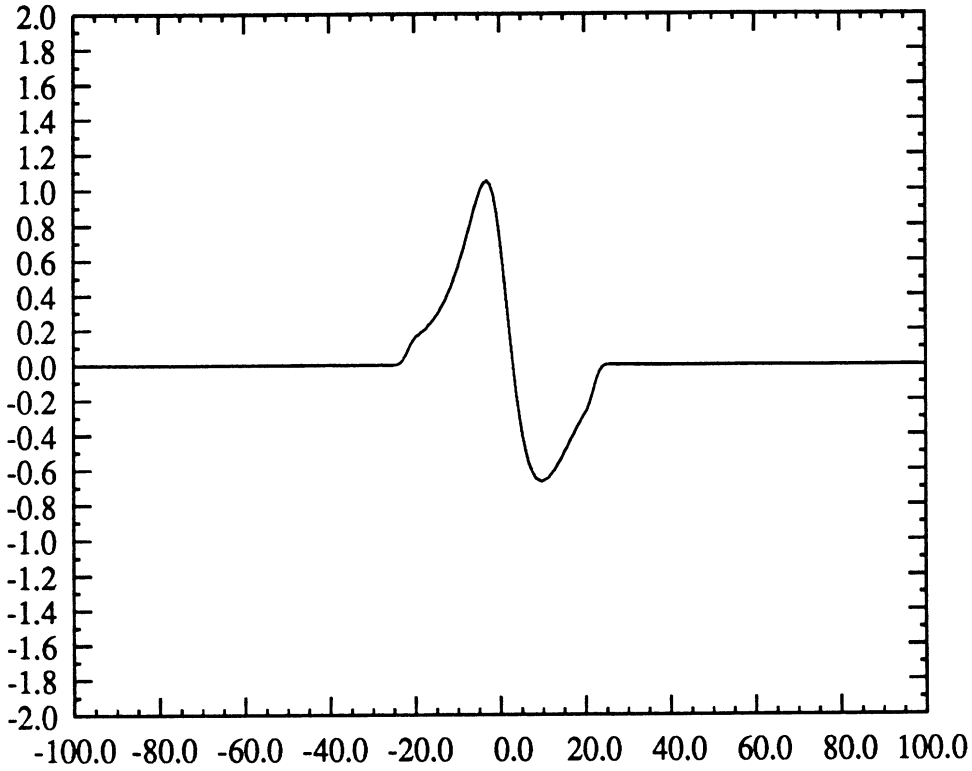

Figure 5. Range profilte attributed to the S-shaped surface obtained by range-gating the profile shown in figure 4b.

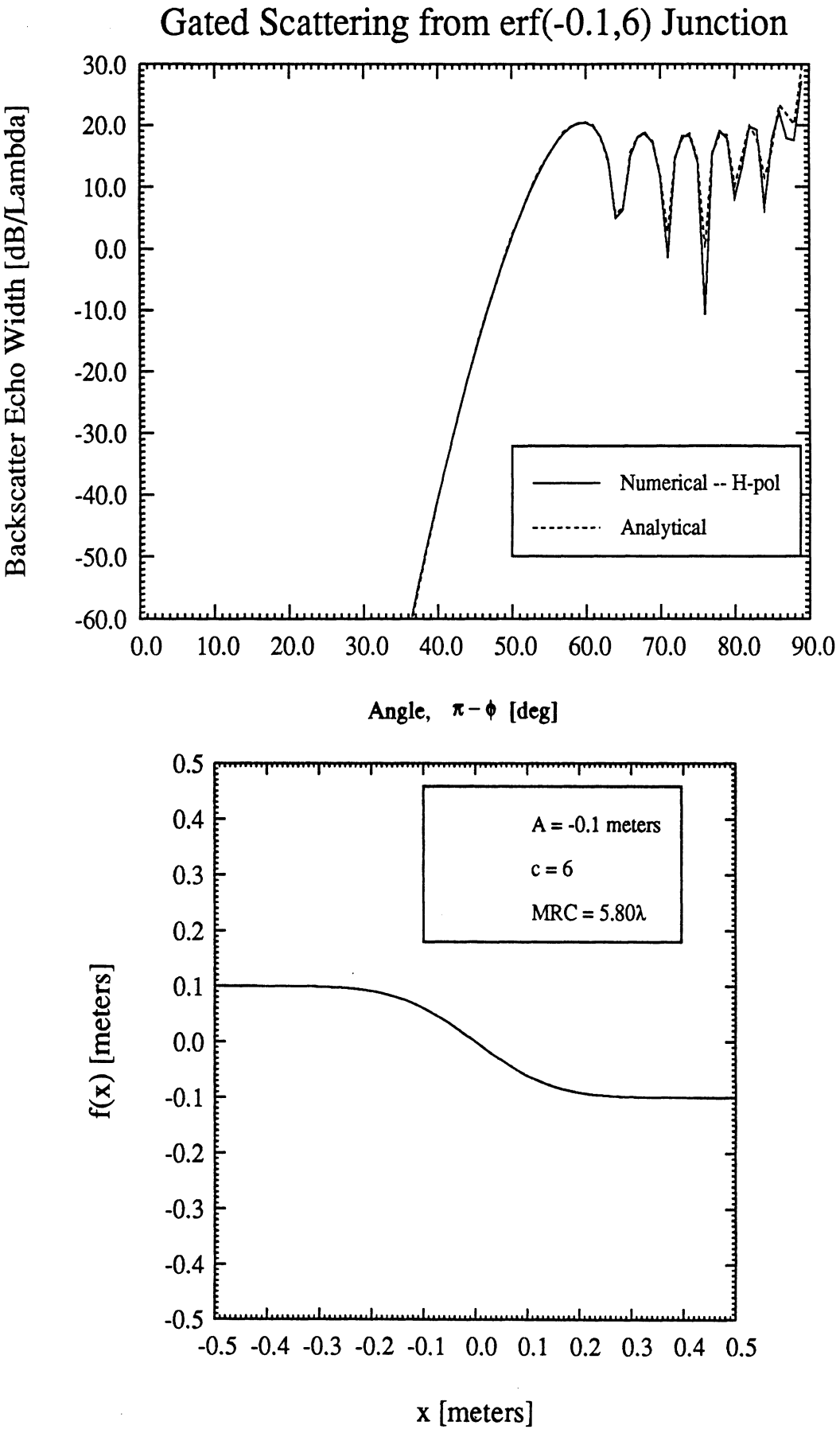

Figure 6. Comparison of backscatter patterns of the illustrated S-shape surface based on the UPO and numerical range-gated solutions (H-pol)

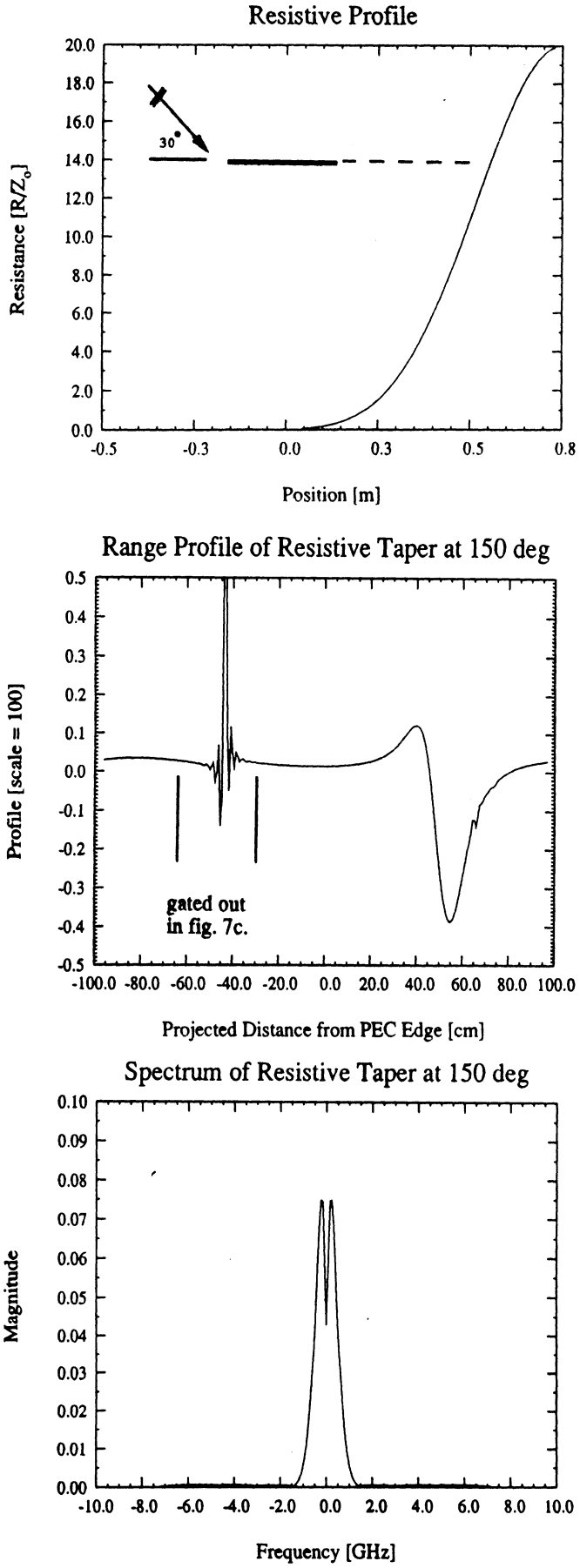

Figure 7. Range profile and the corresponding frequency response of a leading metallic edge terminated with a polynomial resistive taper. (a) profile of resistive taper (inset: geometry) (b) backscatter range profile at 30 deg. off grazing (c) frequency response of range profile with leading edge grated out.

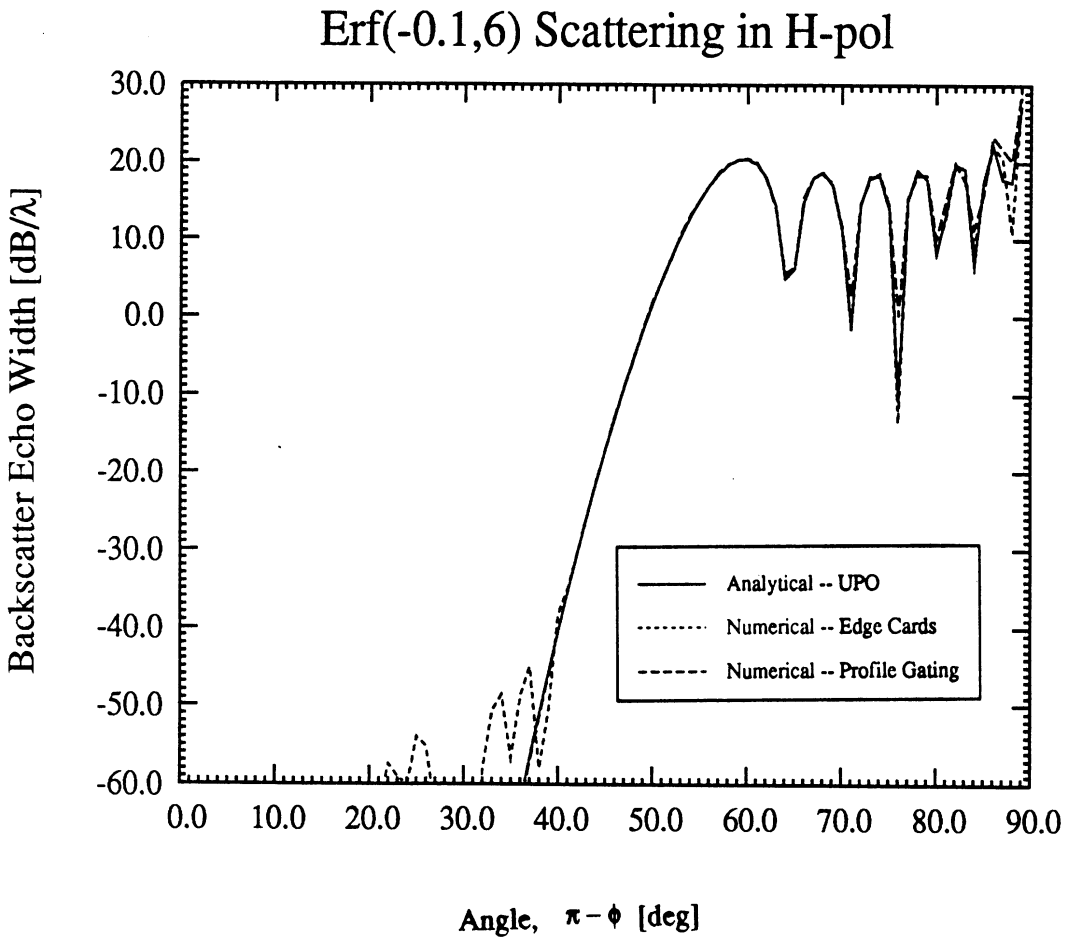

Figure 8. Comparison of H-polarization backscatter patterns for the S-shape surface given in Figure 6 as obtained by three different methods; the analytic UPO solution, the direct numerical solution using the model in fig. 2b and by range gating the results obtained from a model resembling that of fig 2a.

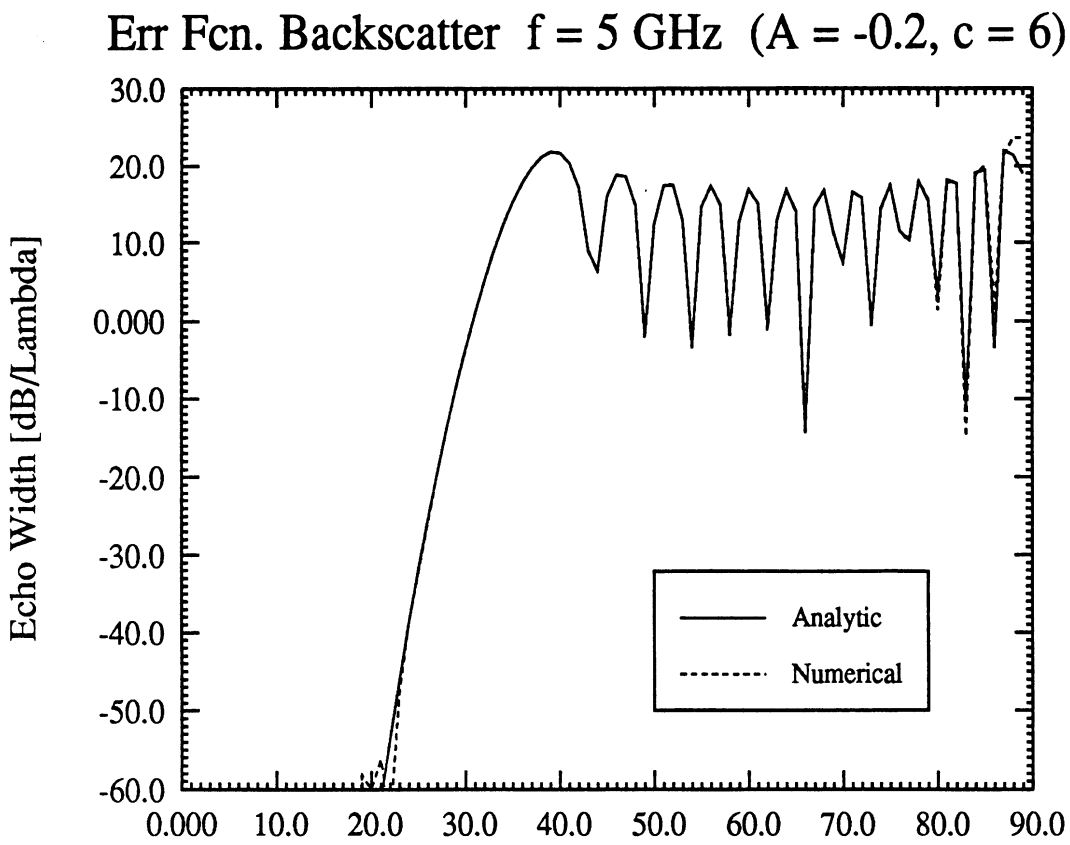

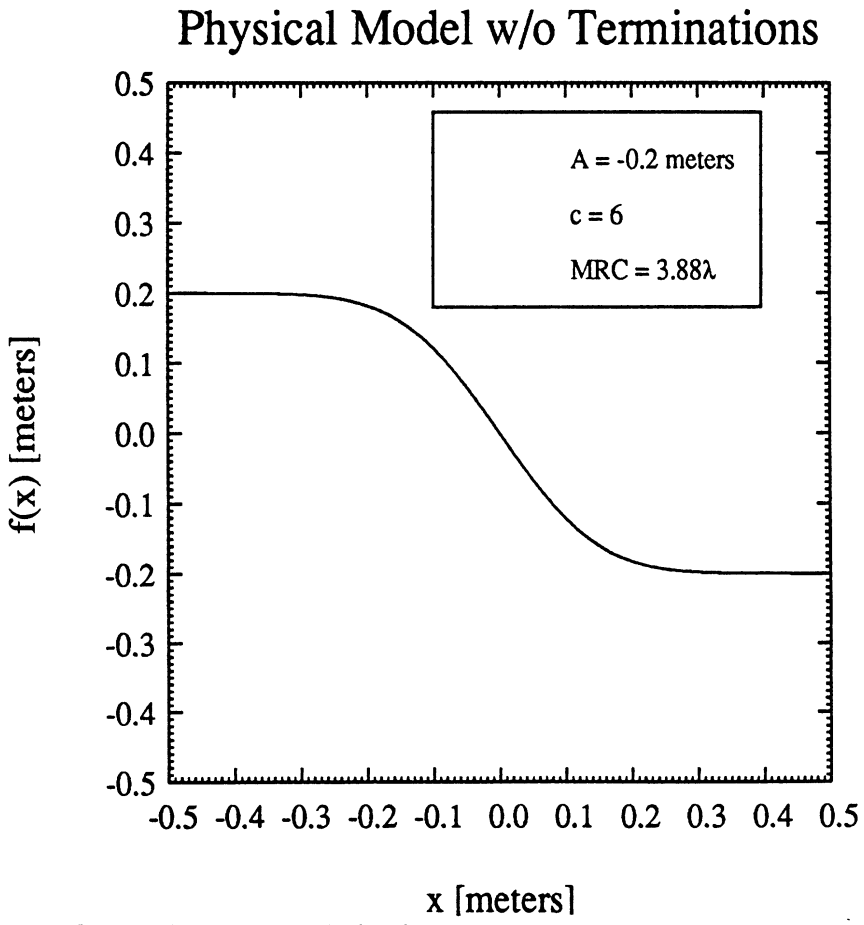

Figure 9. Comparison of H-polarization backscatter patterns of the illustrated S-shape surface based on the UPO and numerical solutions; numerical solution is based on the model in fig. 2b

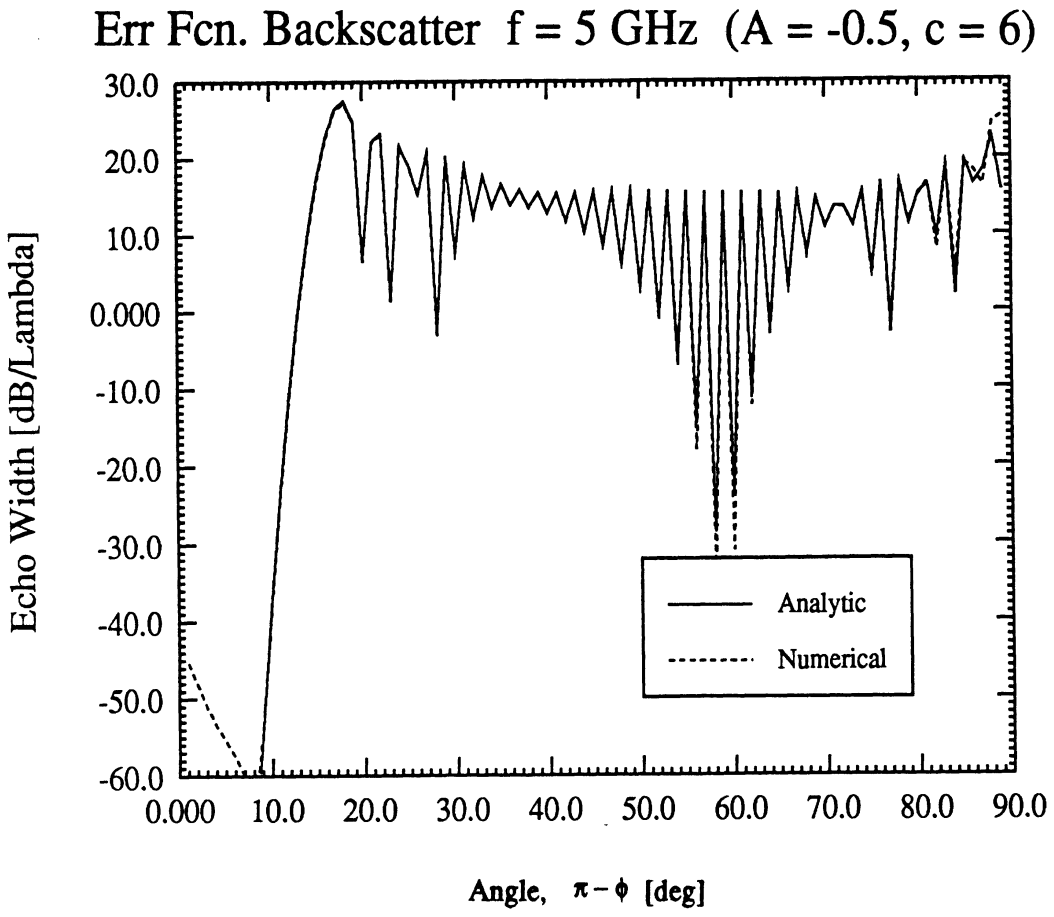
Err Fcn. Backscatter f = 5 GHz (A = -0.5, c = 6)
Echo Width [dB/Lambda]
30.0
20.0
10.0
0.000
-10.0
-20.0
-30.0
-40.0
-50.0
-60.0
0.000
10.0
20.0
30.0
40.0
50.0
60.0
70.0
80.0
90.0
Analytic
Numerical
Angle, π − ϕ [deg]

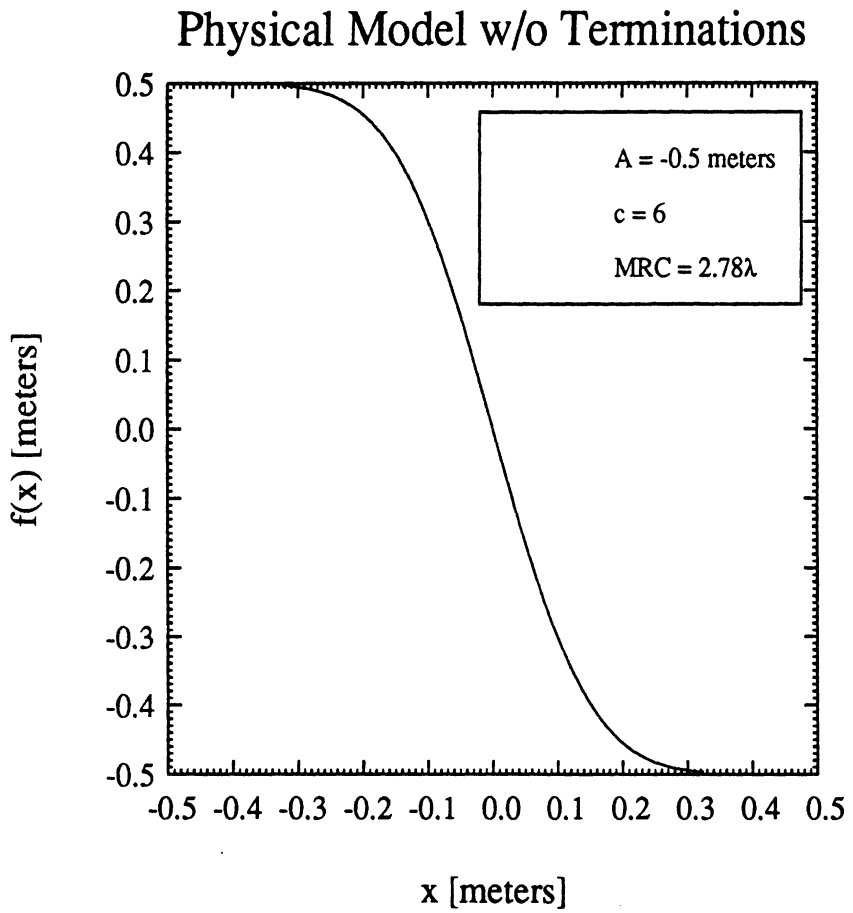
Physical Model w/o Terminations
f(x) [meters]
0.5
0.4
0.3
0.2
0.1
0.0
-0.1
-0.2
-0.3
-0.4
-0.5
-0.5
-0.4
-0.3
-0.2
-0.1
0.0
0.1
0.2
0.3
0.4
0.5
A = -0.5 meters
c = 6
MRC = 2.78λ
x [meters]

Figure 10

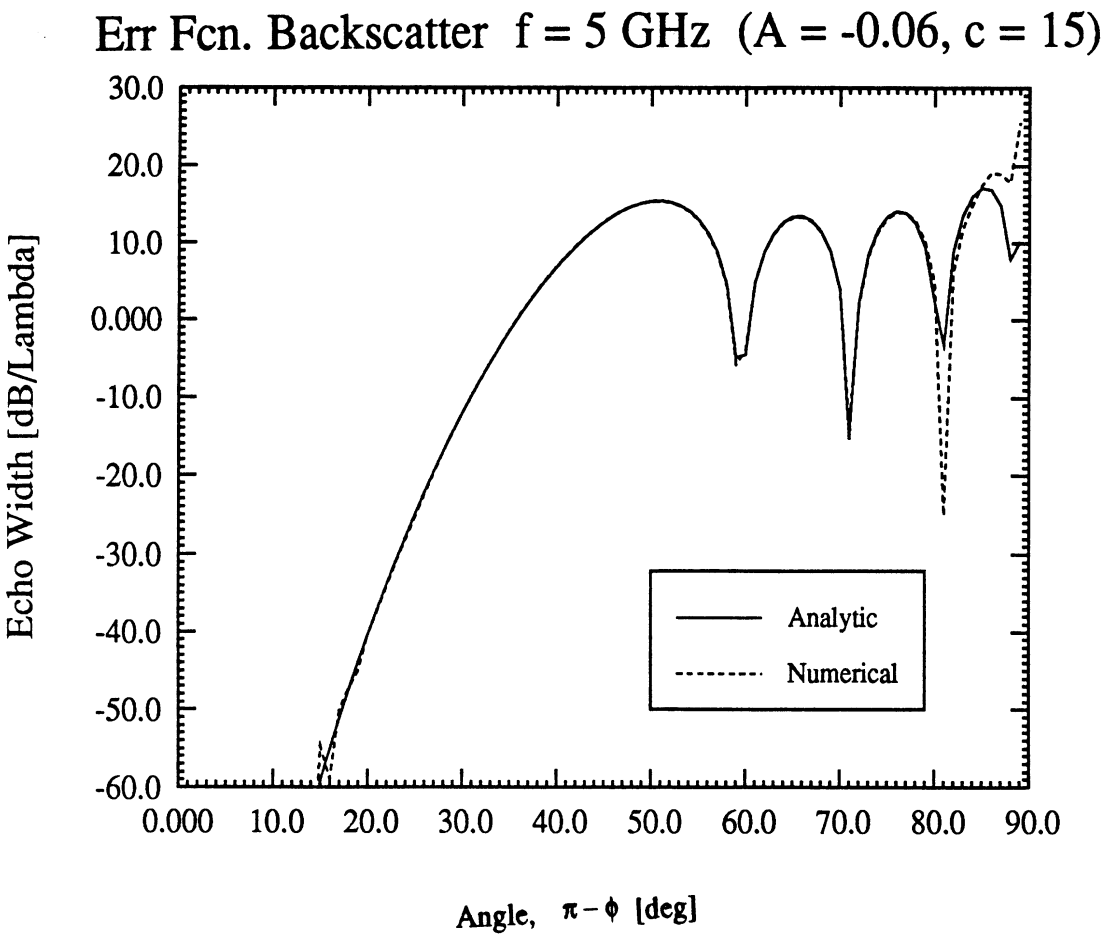
Err Fcn. Backscatter f = 5 GHz (A = -0.06, c = 15)
Echo Width [dB/Lambda]
30.0
20.0
10.0
0.000
-10.0
-20.0
-30.0
-40.0
-50.0
-60.0
0.000
10.0
20.0
30.0
40.0
50.0
60.0
70.0
80.0
90.0
Analytic
Numerical
Angle, π − ϕ [deg]

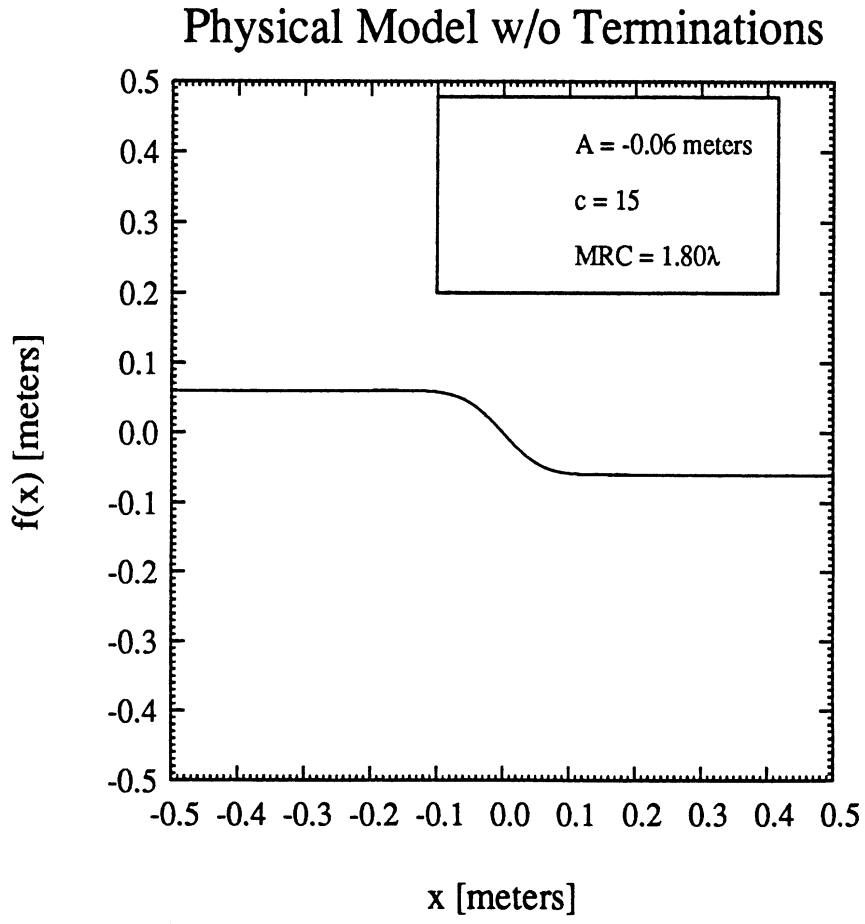
Physical Model w/o Terminations
f(x) [meters]
0.5
0.4
0.3
0.2
0.1
0.0
-0.1
-0.2
-0.3
-0.4
-0.5
A = -0.06 meters
c = 15
MRC = 1.80λ
-0.5 -0.4 -0.3 -0.2 -0.1 0.0 0.1 0.2 0.3 0.4 0.5
x [meters]

Figure 11

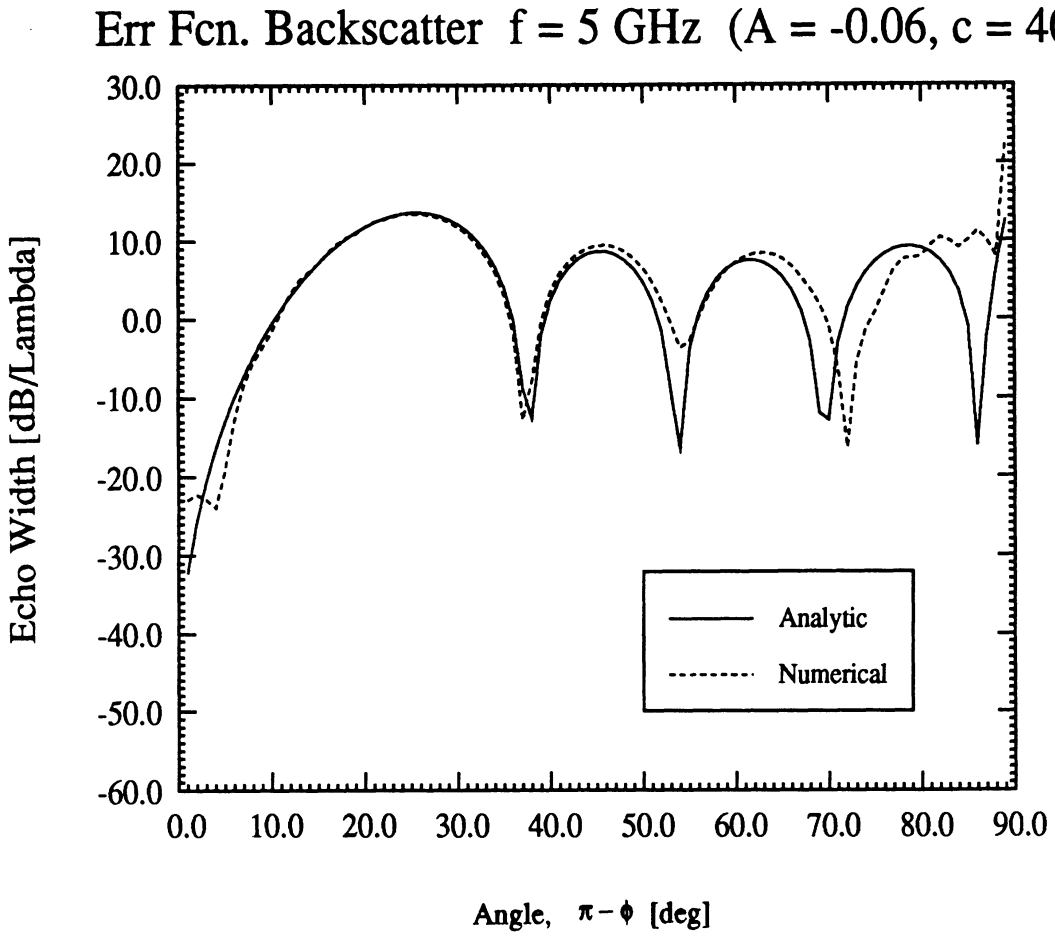
Err Fcn. Backscatter f = 5 GHz (A = -0.06, c = 40)
Echo Width [dB/Lambda]
30.0
20.0
10.0
0.0
-10.0
-20.0
-30.0
-40.0
-50.0
-60.0
0.0
10.0
20.0
30.0
40.0
50.0
60.0
70.0
80.0
90.0
Analytic
Numerical
Angle, π − ϕ [deg]

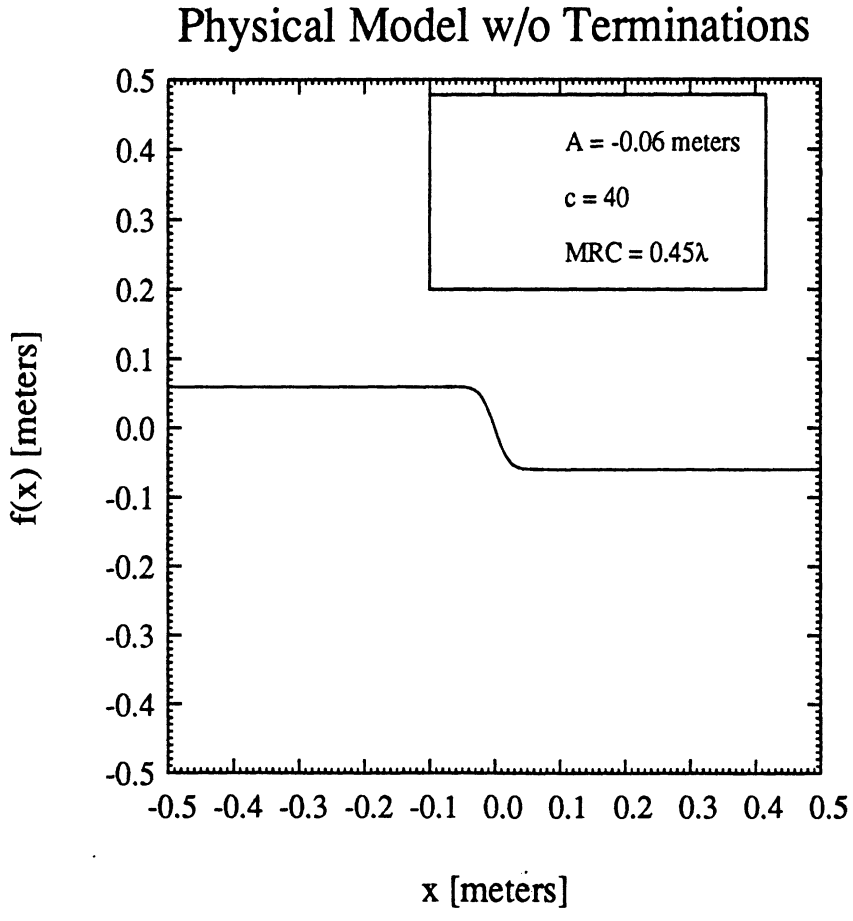
Physical Model w/o Terminations
f(x) [meters]
0.5
0.4
0.3
0.2
0.1
0.0
-0.1
-0.2
-0.3
-0.4
-0.5
-0.5 -0.4 -0.3 -0.2 -0.1 0.0 0.1 0.2 0.3 0.4 0.5
A = -0.06 meters
c = 40
MRC = 0.45λ
x [meters]

Figure 12

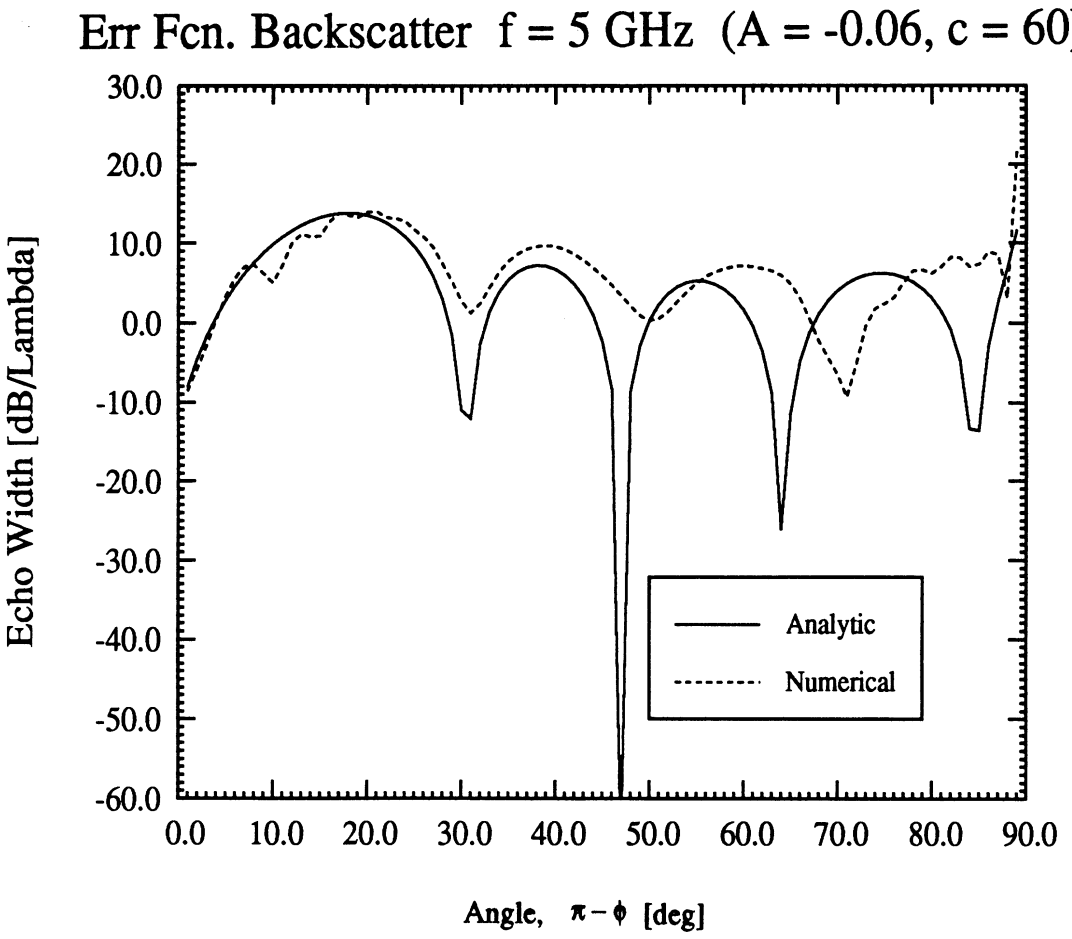
Err Fcn. Backscatter f = 5 GHz (A = -0.06, c = 60)
Echo Width [dB/Lambda]
30.0
20.0
10.0
0.0
-10.0
-20.0
-30.0
-40.0
-50.0
-60.0
0.0
10.0
20.0
30.0
40.0
50.0
60.0
70.0
80.0
90.0
Analytic
Numerical
Angle, π − ϕ [deg]

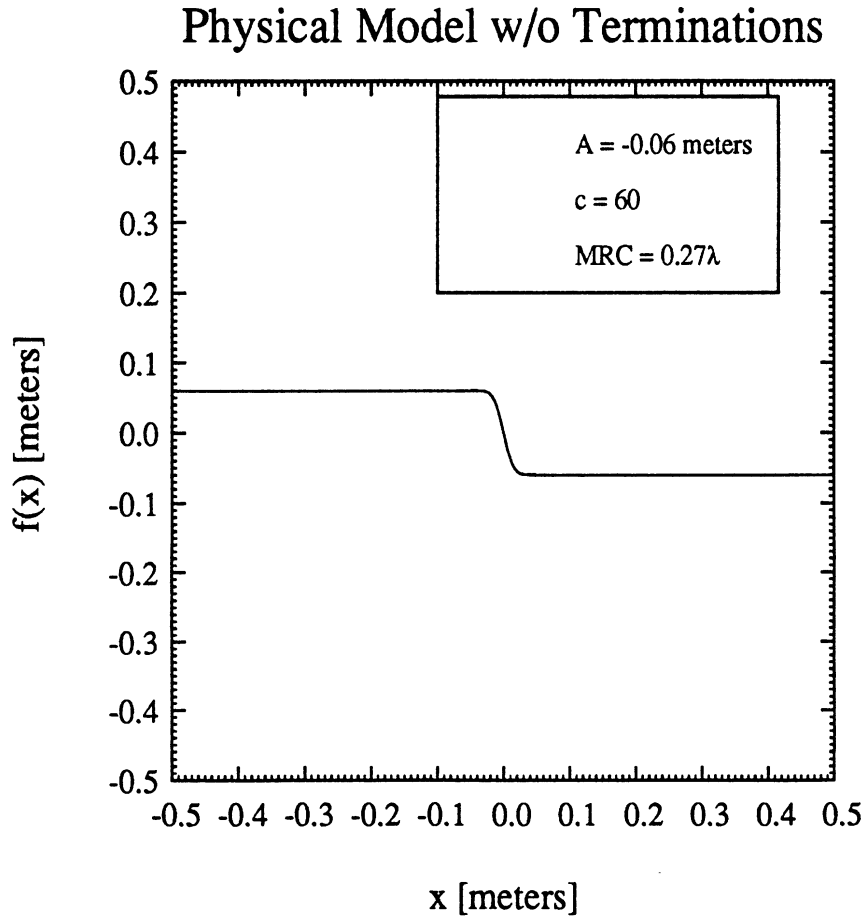
Physical Model w/o Terminations
f(x) [meters]
0.5
0.4
0.3
0.2
0.1
0.0
-0.1
-0.2
-0.3
-0.4
-0.5
-0.5
-0.4
-0.3
-0.2
-0.1
0.0
0.1
0.2
0.3
0.4
0.5
A = -0.06 meters
c = 60
MRC = 0.27λ
x [meters]

Figure 13

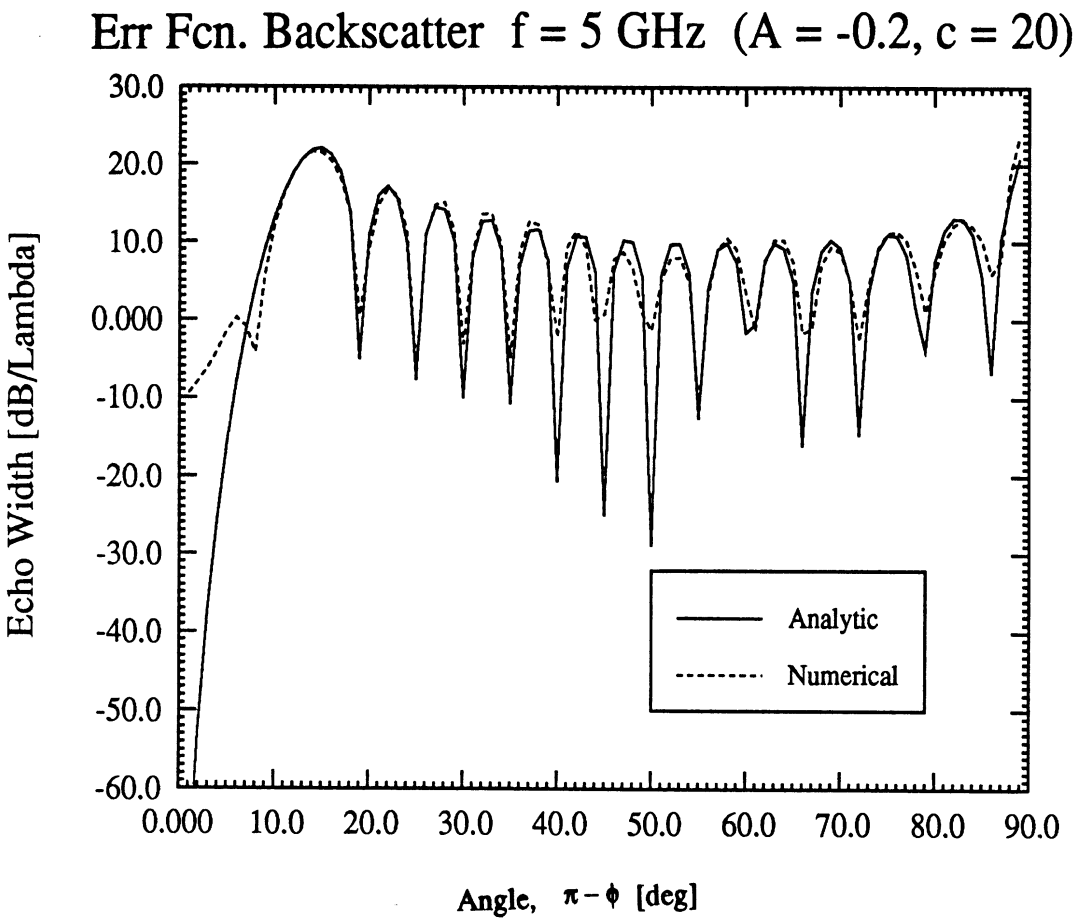
Err Fcn. Backscatter f = 5 GHz (A = -0.2, c = 20)
Echo Width [dB/Lambda]
30.0
20.0
10.0
0.000
-10.0
-20.0
-30.0
-40.0
-50.0
-60.0
0.000 10.0 20.0 30.0 40.0 50.0 60.0 70.0 80.0 90.0
Angle, π − ϕ [deg]
Analytic
Numerical

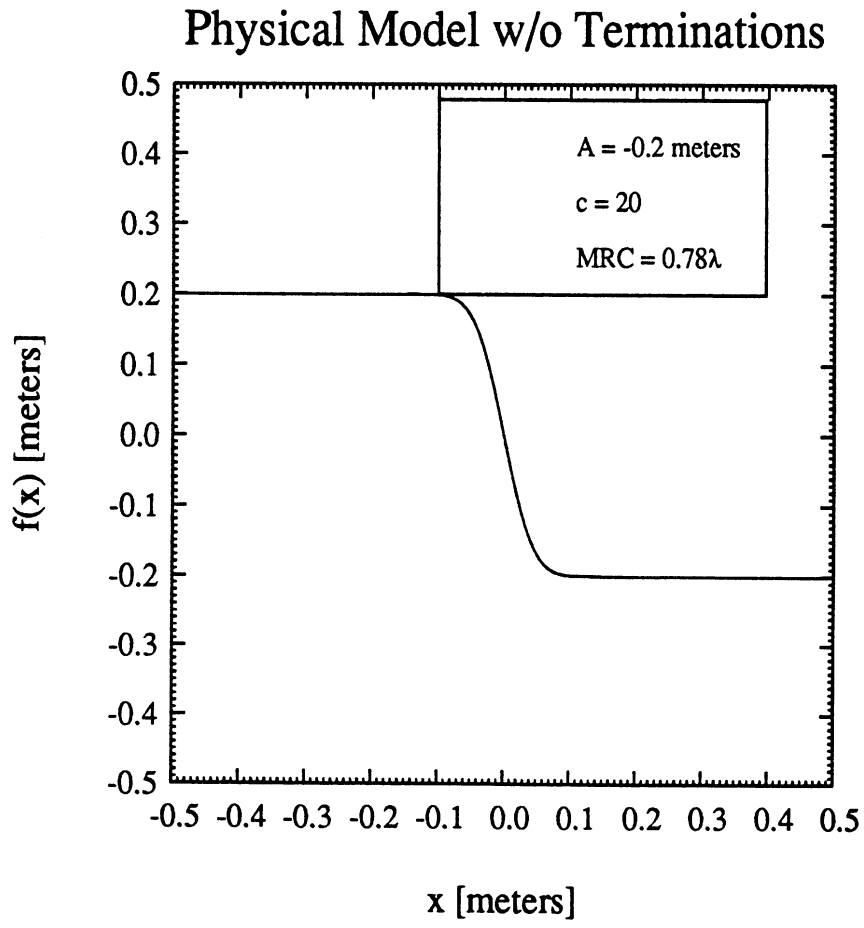
Physical Model w/o Terminations
f(x) [meters]
0.5
0.4
0.3
0.2
0.1
0.0
-0.1
-0.2
-0.3
-0.4
-0.5
-0.5 -0.4 -0.3 -0.2 -0.1 0.0 0.1 0.2 0.3 0.4 0.5
x [meters]
A = -0.2 meters
c = 20
MRC = 0.78λ

Figure 14

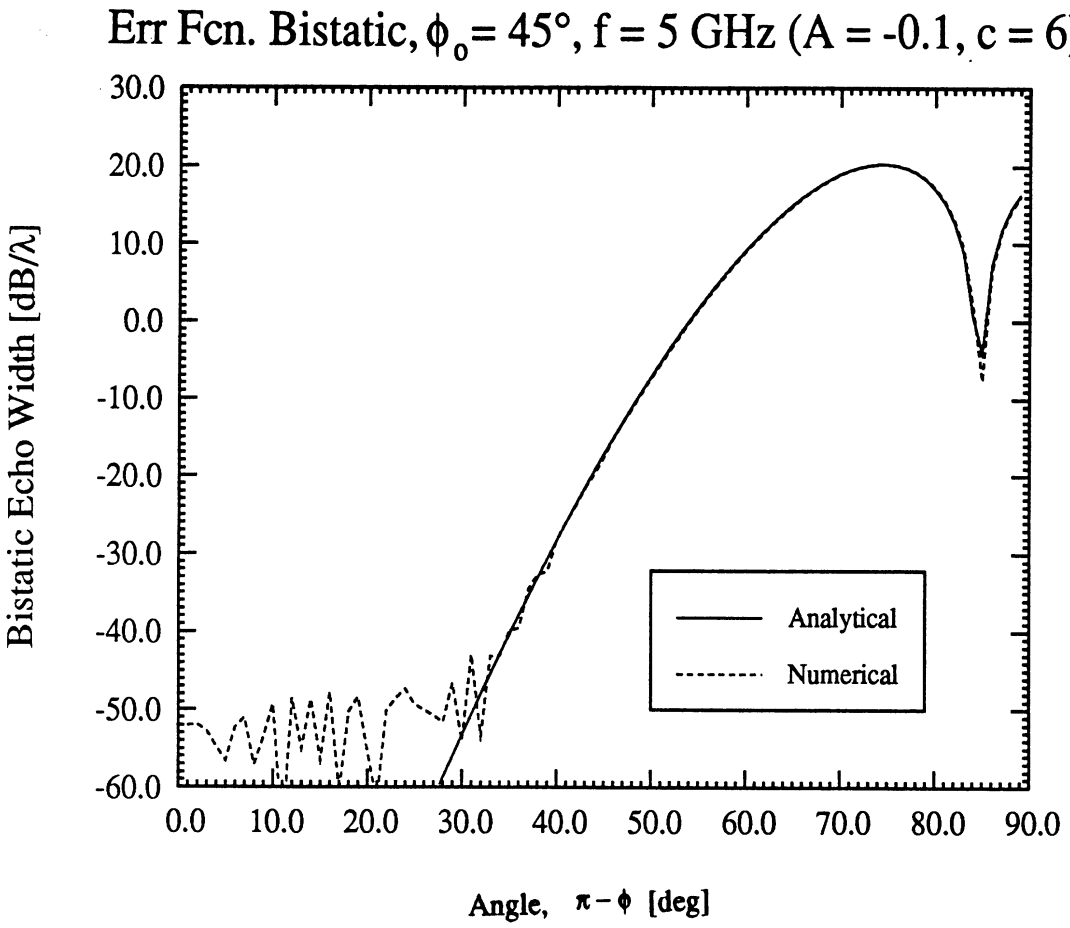

Figure 15 Comparison of E-polarization bistatic patterns of the illustrated S-shape surface based on the UPO and numerical solutions.

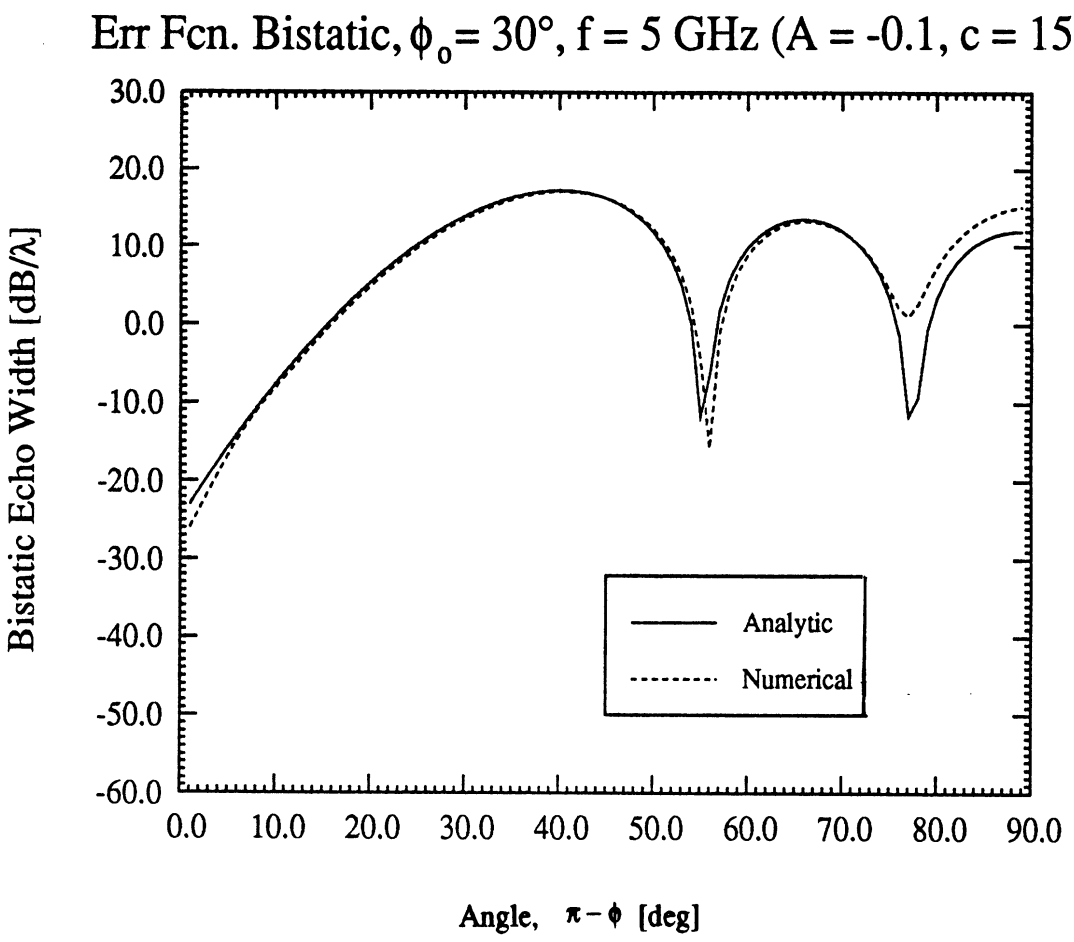

Figure 16. Comparison of E-polarization bistatic patterns of the illustrated S-shape surface based on the UPO and numerical solutions.

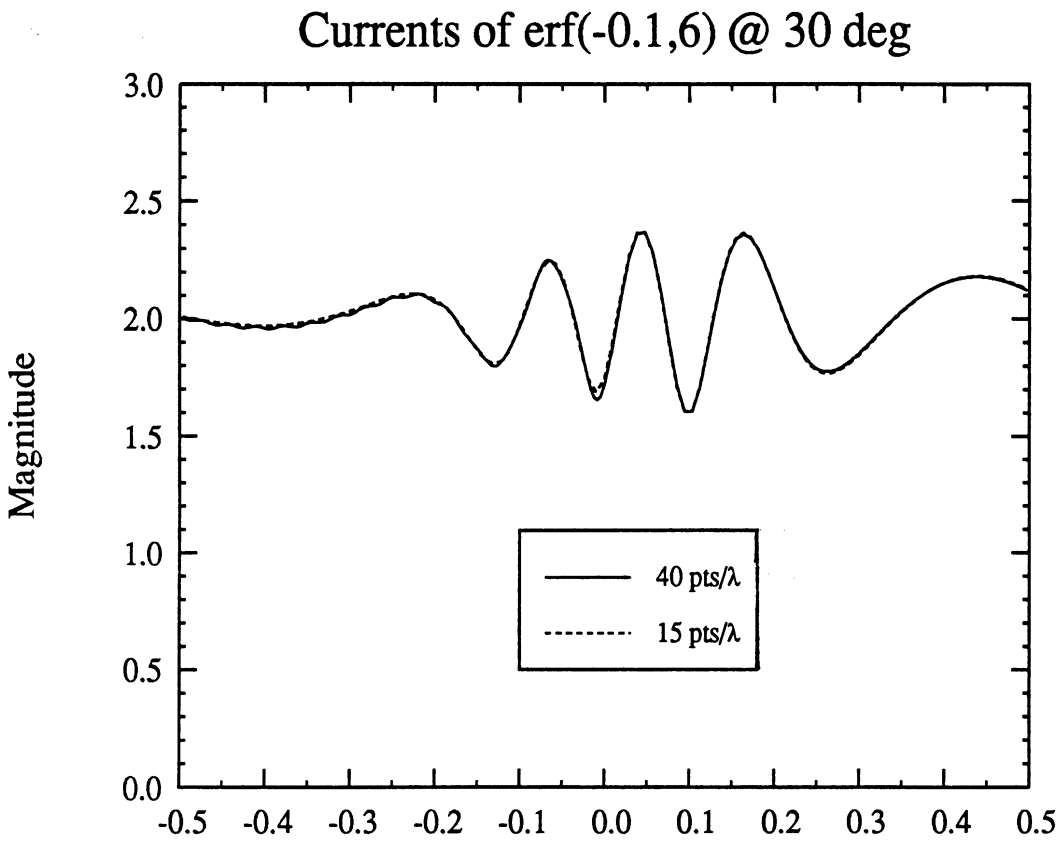

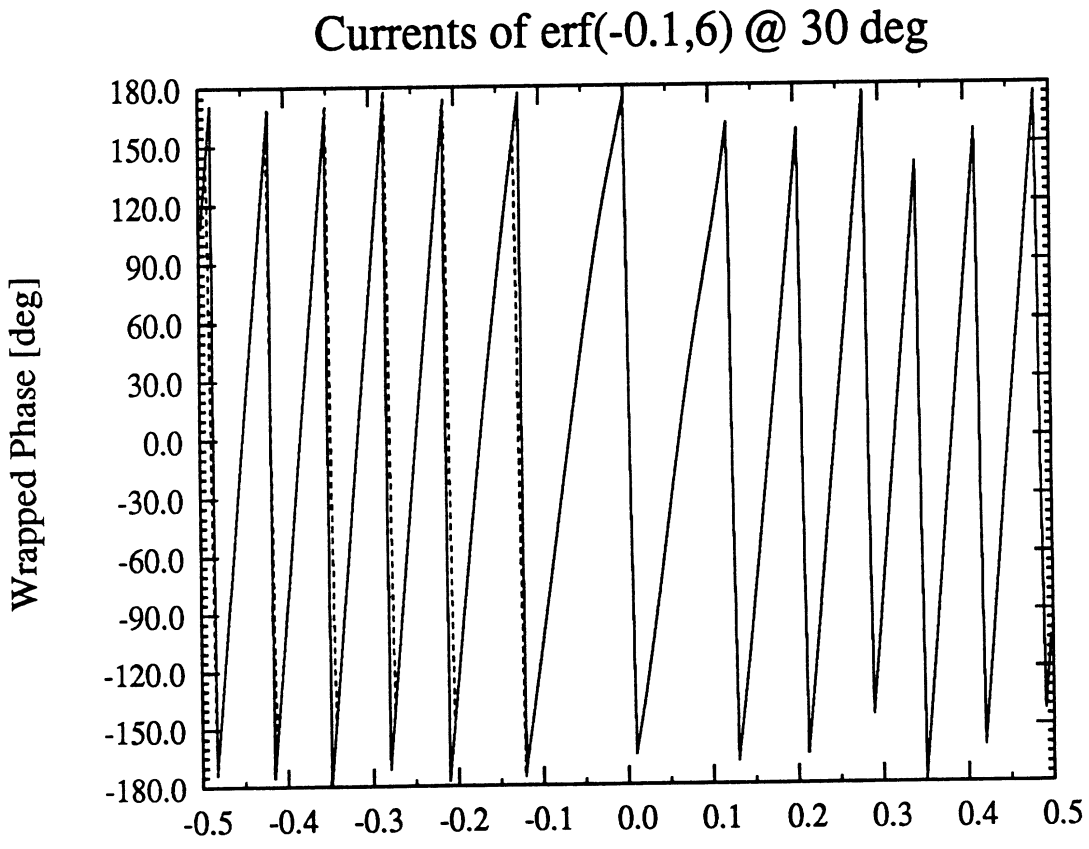

Figure 17. Computed backscatter (30 deg) current of error function model (see fig. 2b) where A = -0.1, c = 6 evaluated at f = 5 GHz in H-polarization
a) Magnitude
b) Phase

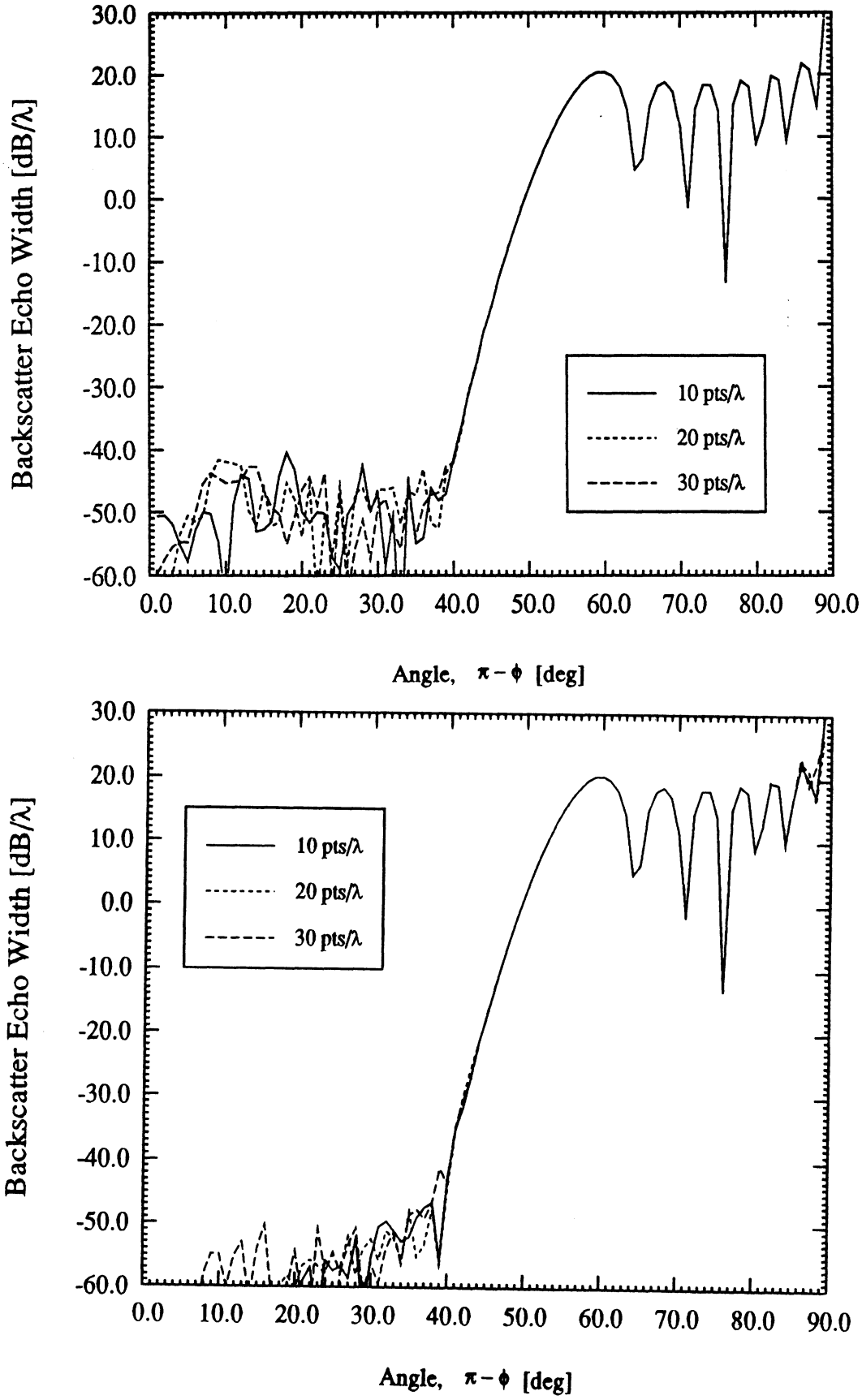

Figure 18. Backscatter patterns of the error function model (A = -0.1, c = 6) evaluated at f = 5 GHz in H-polarization
a) Non-symmetric sampling
b) Symmetric sampling